IOP Publishing Journal of Micromechanics and Microengineering
J. Micromech. Microeng. **17** (2007) 900–908 doi:10.1088/0960-1317/17/5/008

Experimental investigations on the combustion behavior of methane–air mixtures in a micro-scale radial combustor configuration

Sudarshan Kumar[1,3], **Kaoru Maruta**[1] **and S Minaev**[2]

[1] Institute of Fluid Science, Tohoku University, 2-1-1 Katahira, Aoba-Ku, Sendai 980-9577, Japan
[2] Institute of Theoretical and Applied Mechanics, SB-RAS, Novosibirsk, Russia

Received 6 February 2007
Published 3 April 2007
Online at stacks.iop.org/JMM/17/900

Abstract
Experimental investigations on combustion stability limits for methane–air mixtures in a radial micro-scale combustor configuration are herein reported. To study the flame stability characteristics in this radial combustor configuration, two circular quartz plates were arranged parallel to each other and a fuel–air mixture was supplied at the center of the plates. The plates were externally heated to create a positive temperature gradient condition in the flow direction to simplify the heat recirculation process through the solid walls. The fuel–air mixture emanating from the center was subjected to a positive wall temperature gradient and a negative velocity gradient in the radial combustor configuration. Various stable and unstable flame propagation modes were observed during the experimental investigations. The appearance of these modes was a strong function of mixture flow rate, channel width, temperature distribution and mixture equivalence ratio. The effects of wall temperature and mixture equivalence ratios were investigated for a range of mixture flow rates. These investigations showed that the combustion zone moved linearly outward with the increase in the mixture flow rate. At intermediate channel widths (∼2.5 mm), an unstable combustion mode appeared. In this combustion mode, large-scale random fluctuations in flame radius were observed along with the leakage of large amounts of unburnt fuel. Exhaust gas analysis was carried out to compare the combustion performance in stable and unstable combustion modes. Based on the experimental investigations, recommendations are made to facilitate the efficient design of a combustor for micro gas turbine applications.

(Some figures in this article are in colour only in the electronic version)

Nomenclature

b	channel width
d	diameter of the mixture delivery tube
Nu	Nusselt number
r	radial coordinate
Re	Reynolds number
Q	flow rate
SLM	flow rate in standard liters per minute
T_1–T_4	measured wall temperature profiles
U	mixture velocity in the mixture delivery tube
ε	emissivity

[3] Present address: Aerospace Engineering Department, IIT Bombay, Powai, Mumbai 400 076, India.

ϕ	mixture equivalence ratio
μ	viscosity of the fuel–air mixture
ρ	density of the fuel–air mixture

1. Introduction

The availability of compact, highly efficient, durable and high-density power supply systems is becoming increasingly important to improve the quality of our daily life. However, most of these systems, such as cellular phones, notebook computers, portable electronics, micro aerial vehicles and other communication devices are currently powered by electrochemical batteries. These electrochemical batteries have a short life span, long recharging periods and low-energy densities. Therefore, to improve the working cycle and efficiency of these devices, the development of a microscale heat engine for continuous power generation is essential. Combustion-based power generating devices are one of the most promising micro power sources due to higher energy density of hydrocarbon fuels (∼20–50 times) as compared with that of electrochemical batteries [1–4]. There are many other advantages associated with these small-scale combustion-based systems. These advantages include higher heat and mass transfer coefficients and lower pollutant emissions, especially NO_x, due to the lower operating temperature of these systems as compared with those of conventional macro-scale systems [1, 3]. Small-scale combustion-based heaters can be used as efficient heaters for steam reformers in integrated micromechanical systems to produce hydrogen for small-scale fuel cell applications [5]. The increased heat loss due to the large surface area–volume ratio adversely affects the combustion stability limits in these devices. To obtain stable combustion, heat recirculation through solid walls is a key factor for efficient operation of these small-scale devices [6, 7]. In this technique, the solid walls absorb heat from exhaust gases in the downstream region and transfer it to preheat the fresh reactants in the upstream region to enhance the combustion stability limits. Wall thickness and thermal conductivity of solid walls play an important role in determining the heat recirculation performance of the system configuration. A detailed theoretical analysis of these heat recirculation parameters can be found in the literature [6].

A conceptual design for a microscale gas turbine engine has been proposed by the MIT group [8–11]. In this combustor configuration, the fuel–air mixture enters the combustor at the outer periphery. The combustion reaction occurs in the combustion chamber and the combustion products are discharged near the center of the geometry. Experimental investigations on the combustion characteristics of this hydrogen-fueled micro combustor showed stable operation of the combustor under certain operating conditions. However, it has been observed in both experimental and numerical studies that the reaction zone moves upstream and stabilizes near the recirculation jacket for high equivalence ratio [12, 13] and low outer wall heat loss conditions [13]. The flame stabilization in the recirculation jacket leads to higher combustor wall temperatures, thus resulting in higher heat losses and lower thermal efficiency of the combustor. Higher wall temperature also leads to excessive thermal heating which adversely affects the combustor life.

In order to enhance the operation limits of the MIT micro gas-turbine combustor, a modified combustor configuration has been proposed by Wu *et al* [13]. Numerical simulations showed that the overall combustor efficiency (defined as the ratio of actual temperature rise to the maximum possible temperature rise) of the proposed design is about 15% higher (from 61 to 76%) than the original MIT design under two extreme operating conditions of high equivalence ratio and low heat loss through the solid walls. The entry of fresh reactants at the center with a diverging flow field leads to a decrease in the velocity along the flow path. The high velocity in the upstream effectively prevents the flame flashback for high equivalence ratio mixture and low heat loss conditions, thereby creating favorable conditions for combustion and increasing the flame stability limits of the combustor. Guidez [14] and Dumand *et al* [15] have proposed an alternate design of a micro gas turbine combustor and preliminary studies have been carried out with H_2–air mixtures. Another alternate microcombustor configuration for micro gas turbine engines has also been computationally investigated by Verstraete and Trilla [16] for increased flame stability and residence time.

In the present work, a new radial microchannel configuration was chosen, with two circular quartz plates being maintained parallel to each other and a premixed methane–air mixture being supplied at the center. Methane–air mixture is used for detailed investigations which are reported in this paper. Propane and butane–air mixtures were also used in some of the preliminary experiments to examine the flame stabilization behavior of these fuels and these results are reported in [17]. Fuel–air mixture flows radially outward through the microchannel with a flow divergence in the radial direction. This essentially means that the flow area increases linearly with the radial distance which leads to a decrease in the flow velocity and increase in the pressure when scale is extremely small [18]. The flame is expected to stabilize at a location where the flow velocity equals the local flame propagation velocity. This work can also be viewed as an extension of the flame propagation behavior of methane–air mixtures in an extended 2D configuration, when compared with earlier studies on flame propagation in a straight quartz tube (1D configuration) with a positive temperature gradient [4]. A positive temperature gradient in the direction of flow is maintained with external heating to simulate the heat recirculation through the solid walls. The previous one-dimensional study on flame propagation behavior in a straight quartz tube showed the existence of various stable and unstable flame propagation modes over a range of mixture flow rates and equivalence ratios [4, 19]. In the present configuration of a radial microchannel, the fuel–air mixture is simultaneously subjected to a positive temperature gradient and flow divergence since it is important to understand the combined effect of these variables on the combustion behavior of fuel–air mixtures. The understanding of the flame stability limits in the radial microchannel configuration will facilitate an efficient design of micro-combustors and other combustion-based small-scale devices.

The present paper is organized as follows. Details of the experimental setup and different measurement systems are explained in section 2. In section 3, experimental results are presented and various combustion characteristics of the stable

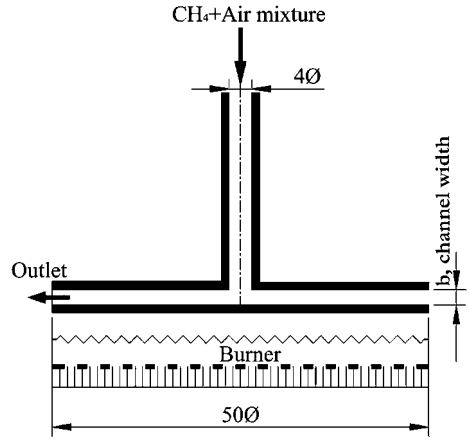

Figure 1. Details of the experimental setup (all dimensions are in mm).

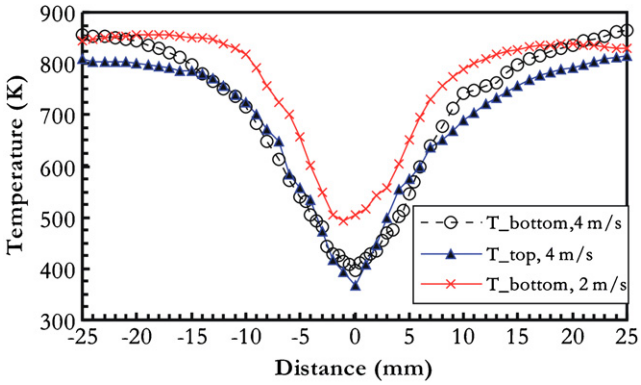

Figure 2. Measured temperature profiles of the top and bottom plates for a channel width of $b = 2.0$ mm at mixture velocities of 2.0 m s^{-1} (1.5 SLM) and 4 m s^{-1} (3.0 SLM) mixture velocities.

combustion mode are discussed. This is followed by a brief summary of the present work on the flame stability limits in small-scale combustors and recommendations for an efficient design of a micro gas turbine combustor.

2. Experimental setup

The schematic of a radial microchannel is shown in figure 1. Two circular quartz plates are maintained parallel to each other within an accuracy of $\pm 0.1^{\circ}$, with the help of a level indicator. The distance between two plates is varied from 0.25 mm to 5.0 mm as described later. The flatness of quartz plates is 0.01 mm per mm. To simulate the heat recirculation process, which has a positive temperature gradient in the flow direction, the circular quartz plates are heated from the bottom with the help of a circular cross-section sintered metal burner. This helps in creating a positive temperature gradient in the radial outward (flow) direction when the mixture is injected at the center through a mixture delivery tube with a diameter of 4 mm. The quartz plates were constantly heated during all the experimental investigations to exclude the effect of varying temperature distribution with heating rate on the observed flame patterns. The temperature profile along the inner side of the quartz plates was measured for air flow conditions with a 300 μm sized K-type thermocouple to study the effect of the flow on the wall temperature profile. The measured temperatures are corrected for radiation heat loss from the thermocouple bead and the corrected temperatures are accurate to ± 5 K of the actual value. A cooling arrangement was incorporated in the mixture delivery tube to maintain the upstream temperature of the incoming mixture. Methane gas of 99.99% purity was used as fuel during the present investigations. Electric mass flow controllers were used to precisely monitor the mass flow rates of methane (0–1 SLM) and air (0–5 SLM) within $\pm 1\%$ accuracy of the full scale. These mass flow controllers were controlled through a digital-to-analog converter board which enabled the independent control of both air and fuel.

The flame visualization studies were carried out with the help of a CCD digital video camera. The recorded images were digitized and detailed features related to flame radius were extracted from these recordings. The uncertainties in the measured flame radius due to various effects are expected to remain less than 5% of the measured values. Exhaust gas analysis was carried out with a 'Shimazdu GC-14B' gas chromatograph. A micro syringe was used to draw a sample of exhaust gases from the combustion zone. A sample of 300 μl was drawn and fed into the gas analyzer. The concentrations of the major species, such as CO_2, CO, CH_4 and O_2 were determined. The uncertainties in the measurements of exhaust gas emissions are less than 3% of the measured values.

3. Experimental results

3.1. Wall temperature profile characteristics

The wall temperature profiles on the inner side of the top and bottom quartz plates were measured in advance with airflow to examine the effects of flow on the wall temperature profile. Figure 2 shows the measured temperature profiles with an airflow velocity of 4 m s^{-1} ($Q \sim 3$ SLM) through the delivery tube. The top plate is heated due to convection and radiation from the bottom plate. Both of these mechanisms play significant roles in the heat transfer between the top and bottom plates. The role of convectional heat transfer mode decreases in the radial direction due to a linear decrease in the Reynolds number ($Nu \sim Re^{1/2}$ and $Re = \rho Q/2\pi\mu r$ $Re \sim r^{-1}$, where Q is the flow rate and r is the radial coordinate). Similarly, the role of radiation was also observed to be significant due to high emissivity of the quartz glass ($\varepsilon = 0.94$–0.96). Therefore, the measured temperatures of both plates are quite similar, with a slightly lower temperature of the top plate (~20–50 K). To quantify the effects of mixture flow rate on the wall temperature profile, wall temperature measurements were carried out over a range of flow rates varying from $Q \sim 1.5$–5.3 SLM ($U = 2$–7 m s^{-1}). The temperature measurements for the bottom wall at a flow rate of 1.5 SLM ($U = 2$ m s^{-1}) are shown in figure 2. It can be concluded from the temperature profiles corresponding to $U = 2$ and 4 m s^{-1} that the temperature gradient increases with the decrease in the flow rate and the peak wall temperature is reached at a smaller radius. Similarly, the temperature gradient decreases with the increase in the flow rate and the peak wall temperature is reached at a larger radius.

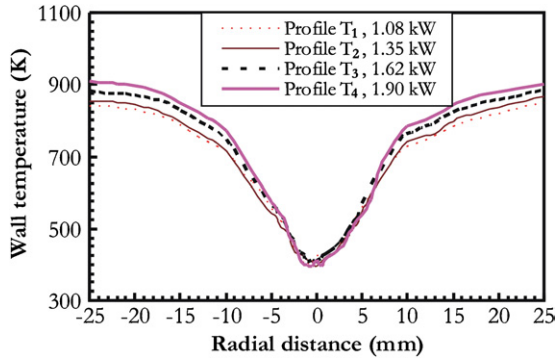

Figure 3. Measured wall temperature profiles of the bottom plate for different thermal inputs of the heating burner for a channel width of 2.0 mm.

The wall temperature profiles T_1–T_4 were obtained for different thermal inputs of the porous burner at 1.08, 1.35, 1.62 and 1.9 kW, respectively, as shown in figure 3. Despite varying the thermal power input of the porous burner by approximately two times, the overall wall temperature variation was approximately 50 K. The increase in the thermal input of the porous burner increased the flame size of the burner. This increased the heat loss from the heating burner and, therefore, the overall rise in the wall temperature was not proportional to the heating rate. The measured temperature profile of the present experiments is similar to that of Maruta *et al* [4, 19] in a straight quartz tube, with a positive temperature gradient in the flow direction. The lowest temperature of 410 K was measured at the center and the highest temperature of 830 K at a radius of 13 mm. The highest measured temperature along with the temperature gradient ($\sim$32 K mm^{-1}) can be used as representative parameters in the present study. These parameters correspond to a T_2 temperature profile and most of the results presented in this paper were obtained for this temperature profile unless otherwise stated.

3.2. Preliminary investigations

Parametric studies were carried out to classify the different stable and unstable flame propagation modes observed in the present experiments. Although, some part of this section has already been published in [20], these details are included here to present the preliminary observations, which are important for understanding and appreciating the combustion behavior of fuel–air mixtures in radial microchannels. Mixture equivalence ratio, channel width and mixture velocity are important parameters which affect the flame stability in radial channels. The mixture flow rates were varied from 1.13 to 5.3 SLM with Reynolds number in the mixture delivery tube varying from $\sim$400 to 1800 ($U \sim$ 1.5–7 m s^{-1}). Reynolds number in the radial channel is much smaller than the mixture delivery tube. For instance, at $U = 7$ m s^{-1}, the mixture tube Reynolds number, $Re_{\text{tube}} = 1800$ as compared to the Reynolds number at radial channel entry, $Re_{\text{entry}} = 450$ and channel exit, $Re_{\text{exit}} = 40$. This indicates that the flow remains laminar in the radial channel and Reynolds number linearly decreases along the radial direction. The present results were limited to 5.3 SLM mixture flow rate ($U \sim 7$ m s^{-1}) because the flow is expected to become turbulent at $\sim$6.78 SLM ($U \sim 9$ m s^{-1}, $Re \sim 2300$) and experimental investigations did not show any significant change in the observed flame behavior for the range of 5.3–6.78 SLM ($U \sim$ 7–9 m s^{-1}). The distance between the two quartz plates was maintained at 5 mm at the start of the experiment. These plates were heated from the bottom with a sintered metal burner and air supply was continued through the radial channel to obtain a positive temperature gradient as shown in figure 3, in the direction of flow. This temperature profile was created due to cooling of the wall near the center. Once the temperature of plates achieved steady state, fuel supply was initiated along with the continued air supply through the delivery tube. The fuel–air mixture was automatically ignited due to high temperature of the chamber walls. After the mixture ignition in the radial channel, the distance between the two quartz plates was reduced by 0.25 mm in each step with the help of a micrometer traverse (0.05 mm resolution) and the measured channel width is accurate within $\pm$0.05 mm. When the fuel–air mixture flows through the mixture delivery tube, a small recirculation zone is formed near the entry zone of the radial channel due to 90° bending of the incoming flow. The size of this recirculation zone varies from 2 to 3 mm and it depends on the flow Reynolds number and channel width [18]. This size is very small compared to the flame location which is stabilized in a zone of fully developed flow. Therefore, this recirculation zone is not expected to affect the flame stabilization behavior or mechanisms in any sense. The following schemes were used to classify the various stable and unstable flame propagation modes.

(1) Flame propagation modes with stable flame front characteristics were assigned to group A (A-stable, A-broken).
(2) Flame propagation modes with unstable behavior were assigned to group B.
(3) Flame located at the radial channel outlet was assigned to group C
(4) Flame stabilized at the mixture delivery tube exit was assigned to group D.

Preliminary visual observations carried out with a CCD video camera are shown in figure 4. Various stable and unstable flame propagation modes were observed over a wide range of operating conditions. In combustion regime A-stable, a stable flame front was located at a radial location as shown in figure 4(*a*). This was the dominant combustion mode observed for $\phi = 0.85$ and higher equivalence ratios. This stable combustion mode disappeared at lower mixture equivalence ratios (for $\phi < 0.75$). The radial location of this flame front was a function of the mixture flow rate, equivalence ratio and the channel width. The mixture equivalence ratio affected the radial position of this stable flame front through the change in burning velocity.

Figure 4(*b*) shows the observed unstable flame propagation mode. In this flame propagation mode, various flame pattern formation modes have been observed by the authors [17, 20]. Various quasi-steady spiral and radial flame propagation modes are observed for lean and rich mixtures [17]. The high-speed images of these spiral and radial flame propagation modes observed at $\phi = 0.85$ for different mixture

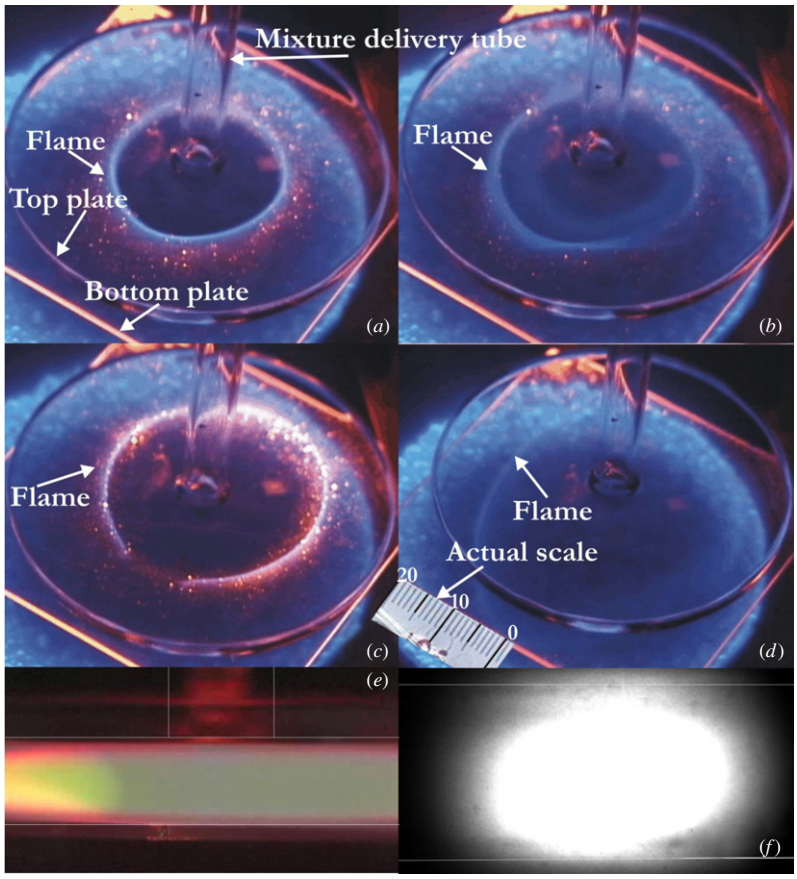

Figure 4. Preliminary observations on various flame propagation modes with a digital video camera. (*a*) A-stable, (*b*) B-regime unstable flame propagation mode, (*c*) A-broken, (*d*) C-regime propagation mode, (*e*) side view of a stable combustion mode, (*f*) side view with a high-speed camera for unstable combustion modes. The white lines in (*e*) and (*f*) indicate the approximate position of the walls.

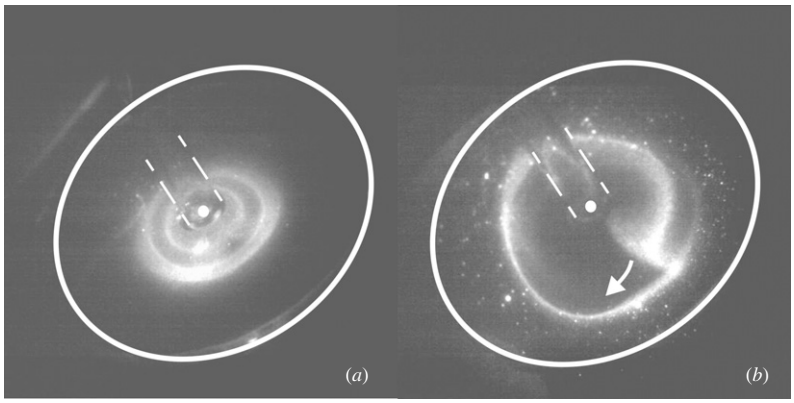

Figure 5. High-speed camera images for radial flame propagation and spiral flame propagation modes in radial microchannels at a condition of $\phi = 0.85$.

velocity conditions are shown in figure 5. These modes are observed for channel widths varying between 2 and 3 mm. Figure 5(*a*) shows the formation of a radial flame propagation mode, where flame instability was generated on the flame front. This flame instability moved in the angular direction along the flame front and developed into a flame kink. This flame kink suddenly ignited the mixture closer to the center and formed a circular ring flame structure at a radius smaller than that of the original flame. This is evident from figure 5(*a*), which shows the simultaneous existence of two circular flames at different radial locations. Alternate layers of reactants and combustion products existed at the interface for very small intervals. Due to the high mixture velocity and low residence time near the center, the inner flame started moving outward. The original flame located at a larger radius weakened over time due to the unavailability of fresh reactants and was finally extinguished. The whole process took 8–10 ms to complete and this cycle recurred after every 30–50 ms.

Figure 5(*b*) shows a spiral flame propagation mode observed at $\phi = 0.85$. In this mode, the flame tip appears to be slightly thickened, which extends toward the center. This is followed by a long, thin tail flame with a length greater than that of the 2π radial. There is an interface of fresh reactants and combustion products. This interface is responsible for the long tail observed in the present experiments. These engulfed reactants keep burning for a longer time and are responsible for the extension of the flame tail beyond the 2π radial length. The flame continuously rotates around the center. The rotational frequency of these rotating modes varies from ∼15 to 100 Hz. The fuel and air mixture leaks from the combustion zone and results in incomplete combustion, which adversely affects the combustion efficiency. However, these rotating flame fronts can also be utilized to generate electric power through the usage of thermoelectric converters because a time averaged uniform temperature distribution is expected.

Figure 4(*c*) shows the A-broken combustion mode. This flame propagation mode generally appears at very small channel widths. The photograph shown in figure 4(*c*) was recorded at $\phi = 0.85$, $Q = 2.26$ SLM ($U = 3$ m s^{-1}) and $b \leqslant 0.25$ mm. At very small channel widths, the stable flame front breaks at one point and this flame extinction point propagates in the angular direction. The precise reasons for the appearance of this propagation mode are unclear at present. A decrease in the channel width increases the mean flow velocity in the radial channel and due to the increase in the mean flow velocity, flame blowout occurs at the weakest point. Due to increased flow velocity, the heat loss from the walls increases and hence, the mean temperature of the walls is not high enough to support a stable flame at this particular location (reduced residence time due to increased flow velocity compared with the increased chemical reaction time due to decreased wall temperature). This leads to an increase in the heat losses from the stable flame, finally leading to complete flame extinction in the micro combustor.

Figure 4(*d*) shows the combustion regime C, which is observed at high velocity and large channel widths. In this regime, a stable flame front with an unsymmetrical flame shape is located near the outer edges of the circular plates. This mode is generally observed at large channel widths (>4 mm) and higher mixture flow rates (>3.77 SLM, $U >$ 5 m s^{-1}). In this mode, the visibility of the flame front is very low. This mode can be compared to the blow-off limit of the combustor at higher mixture velocities. Regime D is generally observed at low mixture flow conditions (<1.5 SLM, $U <$ 2 m s^{-1}) and higher equivalence ratios. In this mode, a stable flame exists at the exit of the mixture delivery tube and resembles to a flame stabilized at the outlet of a straight tube. This condition is similar to a flame flashback and can be equated to the lower operating limit of the present combustor. The presence of the flame at the mixture delivery tube exit results in the breakdown of the positive temperature gradient in the direction of flow due to the existence of a high temperature flame zone near the center.

Figure 4(*e*) shows the side view of the flame in a radial channel for a stable combustion mode. In this mode, the flame appears to be equally attached to both the walls. White lines are drawn to indicate the approximate position of the quartz plates and mixture delivery tube. Figure 4(*f*) shows the side view of the propagating flame front for an unstable combustion mode and this frame is recorded with the help of a high-speed video camera. From these high-speed movies, it appears that the flame is attached comparatively more to the bottom plate than the top plate during the unstable combustion mode.

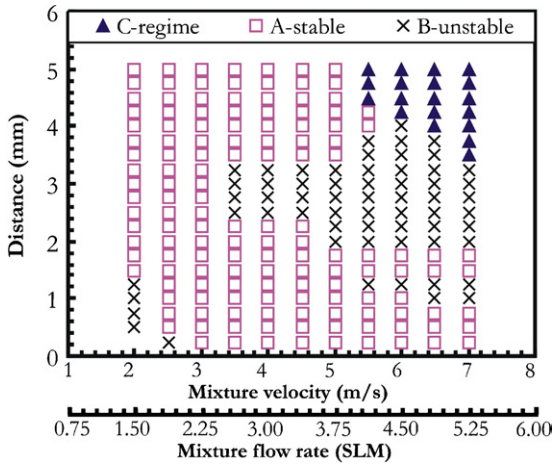

Figure 6. Regime diagram for different combustion modes at $\phi = 0.85$ for T_2 (1.35 kW) temperature profile.

3.3. Combustion regime diagram

Experiments were carried out over a wide range of mixture equivalence ratios for methane–air mixtures. These investigations were carried out at $\phi = 0.67$, 0.85, 1.0, 1.2 and 1.25 with T_2 as a reference temperature profile. These investigations showed that the overall flame propagation behavior remained almost similar for $\phi \geqslant 0.85$. Therefore, a regime diagram was constructed for $\phi = 0.85$, from which it was possible to extract broad features of the stable and unstable combustion modes. For lower equivalence ratios, for instance $\phi = 0.67$, most of the regime diagram was dominated by unstable flame propagation modes and the details of these modes were discussed in the previous section. Figure 6 shows a detailed combustion regime diagram for lean methane–air mixtures at $\phi = 0.85$. This figure shows a strong dependence of channel width and mixture flow rates for different stable and unstable flame propagation modes. The A-stable flame propagation mode dominates the regime diagram for $\phi = 0.85$ and higher equivalence ratios. The presence of unstable flame propagation modes at intermediate channel widths and higher mixture flow rates is noteworthy. The observation of various unstable and rotating flame propagation modes at lower equivalence ratios (at $\phi = 0.67$) suggests that it is difficult to achieve stable combustion at a small scale due to restricted stability limits on the leaner sides. Compared with unstable flame propagation modes at low equivalence ratios, a stable combustion mode can be obtained under a wider operation range of mixture flow rate for $\phi \geqslant 0.85$.

3.4. Variation of flame radius with channel width

Figures 7(*a*) and (*b*) show the variation of flame radius with mixture flow rates for a stoichiometric methane–air mixture at different channel widths, $b = 1.0$, 1.5, 2.5 and 4.5 mm. The

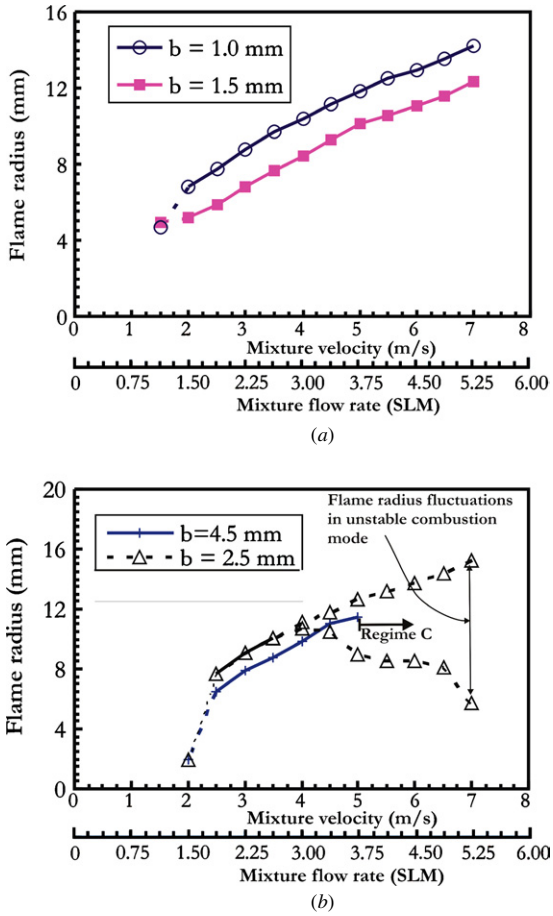

Figure 7. (*a*) Variation of the flame radius for channel widths for 1 and 1.5 mm at $\phi = 1.0$ and T_2 (1.35 kW) temperature profile conditions. (*b*) Variation of flame radius for channel widths of 2.5 and 4.5 mm at $\phi = 1.0$ and T_2 (1.35 kW) temperature profile conditions.

bold lines indicate the flame radius in the stable combustion regime and the dashed lines indicate either the appearance of an unstable combustion regime or flame flashback and flame blowout conditions. In the stable combustion mode, the flame radius increases as the channel width decreases; this can be concluded from figure 7(*a*). The flame radius shows a nearly linear dependence on the mixture flow rate for both 1 mm and 1.5 mm channel widths. At very small mixture flow rates ($Q <$ 1.5 SLM, $U < 2$ m s^{-1}), an unstable flame propagation mode appears for 1.0 and 1.5 mm channel widths. Therefore, it is essential to identify the limits of the stable combustion mode to avoid a sudden appearance of an unstable combustion mode or flame flashback in the combustor.

Figure 7(*b*) shows the variation of flame radius for channel widths of 2.5 and 4.5 mm. As expected, the flame radius varies linearly with the mixture flow rate for the case of 4.5 mm channel width. At higher mixture flow rates, regime C appears where the flame acquires an unsymmetrical shape. It is located at the channel outlet, which can be equated to a condition similar to the flame blowout at higher flow rates. Another condition of 2.5 mm was chosen to show the characteristics of unstable combustion mode in the radial micro-combustor. The upper and lower limits of the curve show the fluctuations in

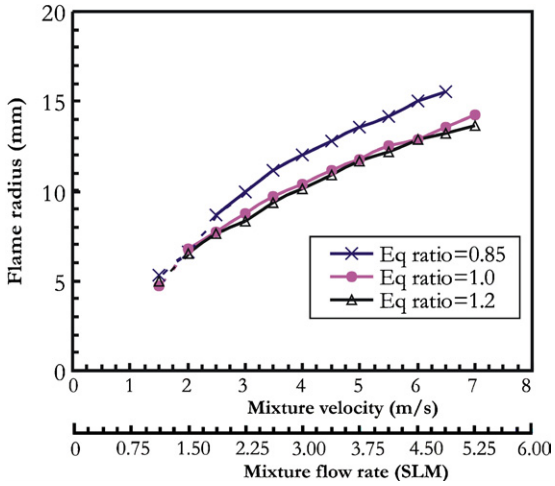

Figure 8. Variation of the flame radius with mixture velocity at different equivalence ratios for T_2 temperature profile and $b =$ 1.0 mm.

the flame radius for different mixture flow rates. Stable flame behavior appears at a flow rate of approximately 2.64 SLM ($U \sim 3.5$ m s^{-1}) and finally regime D appears at a flow rate of 1.5 SLM flow rate ($U \sim 2$ m s^{-1}), where flame flashback occurs and the flame attaches to the outlet of the mixture delivery tube. It is clear from figures 7(*a*) and (*b*) that the flame radius decreases with the increase in the channel width. An unstable flame propagation mode is observed for intermediate channel widths. Therefore, careful consideration of the flame radius and stable combustion mode is important for deciding the combustor size based on the total power requirements.

3.5. Variation of the flame radius for various equivalence ratios

Figure 8 shows the variation of the flame radius with mixture flow rates for different mixture equivalence ratios. A channel width of 1 mm was maintained between the two plates and flame behavior was observed with a CCD video camera and later extracted from the recordings at various operating conditions. The bold lines indicate the radius of the stable flame front and the dashed lines indicate the approximate inner flame radius in the unstable combustion mode. For $\phi = 0.85$, the flame radius is much larger than the flame radius at $\phi =$ 1.0 and 1.2. The flame radius is almost same for $\phi = 1.0$ and 1.2 over a range of mixture flow rates. The flame radius increases monotonously with the increase in the mixture flow rate for different mixture equivalence ratios. For small flow rate conditions, the stable flame propagation mode disappeared and an unstable flame propagation mode appeared in the radial channel. During these unstable flame propagation modes, various flame fronts appeared in the experimental domain. These flame fronts either oscillated in the radial/angular direction or rotated around the center of the mixture source at a frequency of about 15–100 Hz [17, 20]. This could lead to leakage of the unburnt fuel from the combustion zone and incomplete combustion with increased pollutant emissions and lower combustion efficiency.

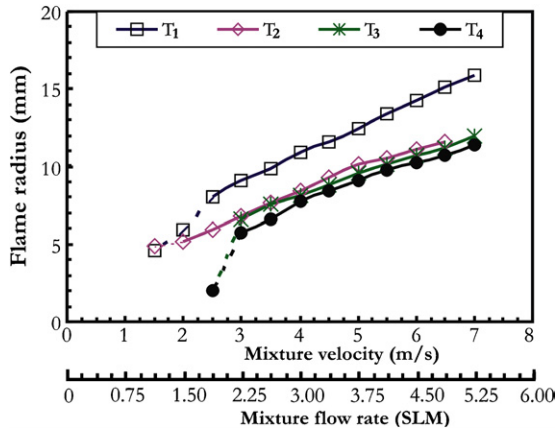

Figure 9. Variation of the flame radius for different temperature profiles at $\phi = 1.0$ and $b = 1.0$ mm.

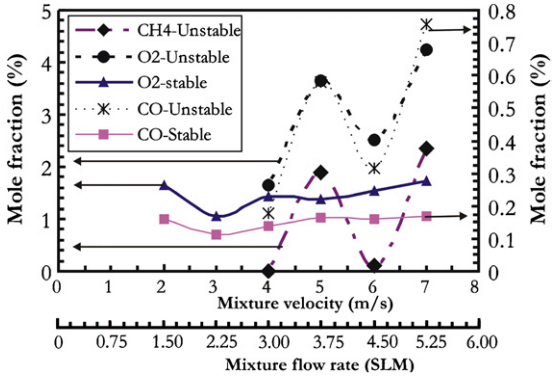

Figure 10. Exhaust gas analysis for stable ($b = 1.5$ mm) and unstable ($b = 2.5$ mm) combustion modes in the radial micro combustor configuration.

3.6. Variation of the flame radius for various temperature profiles

Figure 9 shows the variation of the flame radius for various temperature profiles. These temperature profiles were obtained through different thermal inputs of the porous heating burner. The details of these temperature profiles and the respective thermal inputs to the porous burner are presented in figure 3. Two quartz plates were maintained at a distance of 1.5 mm, and a stoichiometric methane–air mixture was supplied to examine the effect of the temperature profile and peak temperature on the combustion behavior in the radial channel. The bold lines indicate the variation of the flame radius in the stable combustion mode and the dashed lines show transition into an unstable flame propagation mode, which was observed at smaller flow rates. The flame radius varied almost linearly with the mixture flow rate for all temperature profiles as shown in figure 9. It is interesting to note that the flame radius for the T_1 temperature profile is much larger than the flame radius for T_2–T_4 temperature profiles. The flame radius variation from T_2–T_4 temperature profiles is relatively small despite the fact that wall temperature for the T_4 temperature profile is about 50 K higher than T_2. For temperature profiles T_1 and T_2, an unstable flame propagation mode appeared and the flame radius for these unstable modes was approximately 5 mm. For T_3 and T_4 temperature profiles, a flame flashback was observed when the mixture flow rate was changed from 2.26 SLM to 1.88 SLM ($U \sim 3$ m s^{-1} to 2.5 m s^{-1}) and a stable flame was observed to exist at the outlet of the mixture delivery tube (4 mm diameter). The flame behavior at smaller flow rates needs careful consideration due to the appearance of an unstable combustion mode because this transition at smaller flow rates leads to flame flashback in the combustor.

3.7. Exhaust gas analysis

The emission characteristics of the radial combustor configuration were measured for stable and unstable combustion modes. The emission characteristics were measured for stable combustion mode with a channel width of 1.5 mm and stoichiometric methane–air mixtures. For the measurement of emission characteristics in the unstable combustion mode, a channel width of 2.5 mm was maintained (regime diagram in figure 6 shows various stable and unstable combustion modes for various channel widths). The emission characteristics were compared for these two conditions to emphasize that the unstable combustion mode leads to incomplete combustion and reduced combustion efficiency. The concentrations of major species such as CO, O_2 and CH_4 were measured for stable and unstable combustion modes as shown in figure 10. For the stable combustion mode, the variation of CO and O_2 concentration is comparatively small in the whole operating range. CH_4 emissions are not observed for the stable combustion mode, which indicate that there is no leakage of the fuel from the combustion zone. However, for an unstable combustion mode, the average CO emissions are two to three times higher than the emissions from the stable combustion mode. The CH_4 emission profile for the unstable combustion mode shows that large quantities of unburnt methane fuel are detected in the exhaust stream. This is due to the fact that during the unstable combustion mode, single/multiple flame fronts were observed to rotate around the center of the plates [17, 19] and this led to a leakage of combustible mixture. This fact has been proved by the exhaust gas analysis for both stable and unstable combustion modes. Flame extinction near the solid walls is another possible reason for the leakage of unburnt fuel from the combustion zone. The combustion efficiency or chemical conversion efficiency was calculated from the measured emissions and it was found to be ∼99% and ∼67% respectively for stable and unstable combustion modes. Therefore, to summarize, a careful consideration of the operating characteristics is essential to determine the flame stability limits in small-scale combustors. The operating limits of the combustor should be carefully chosen in the stable combustion regime to obtain efficient, clean and stable combustion.

4. Conclusions

Flame stability limits were experimentally investigated in a radial micro-combustor configuration. These investigations were carried out with methane–air mixtures for a wide range of operating conditions by varying mixture flow rate, equivalence ratio, channel width and wall temperature profiles. The investigations showed the existence of both stable and unstable flame propagation modes for different conditions of mixture

flow rate, channel width and mixture equivalence ratios. The measurements of the flame radius showed that it increased linearly with increasing mixture flow rates. At intermediate channel widths, an unstable flame propagation mode was observed. In this mode, the flame behavior was observed to be chaotic in nature, which led to the formation of various rotating flame patterns. The exhaust gas analysis showed that the level of emissions was much higher for the unstable combustion mode due to significant leakage of unburnt fuel. Therefore, the following points should be considered while designing a new microcombustor for micro gas turbine applications.

(1) A radial microcombustor configuration is more advantageous due to its enhanced operating limits and increased combustion efficiency in the stable combustion mode for various hydrocarbon fuel–air mixtures.
(2) Combustor wall temperature, flow rate and mixture equivalence ratio significantly affect the flame stability in a micro combustor. The role of these parameters is very crucial in the design of a new microcombustor and they should be carefully examined while developing a new microcombustor.
(3) Appearance of the unstable combustion mode at intermediate channel widths (∼2.0–3.0 mm) impairs the combustor performance due to incomplete combustion and therefore, combustor operation in this zone should be avoided as it results in a considerable (as high as 32% in the present case) loss of combustion efficiency. The channel width should be chosen carefully to obtain a stable combustion mode in which fuel burns with maximum combustion efficiency.

Acknowledgments

The authors would like to thank Professor S Maruyama, IFS for having useful, interesting and thought-provoking discussions while carrying out this work. They would also like to thank Mr S Hasegawa for helping in the experimental setup and giving useful suggestions for conducting the present experiments.

References

[1] Fernadez-pello A C 2002 Micro-power generation using combustion: Issues and approaches *Proc. Combust. Inst.* **29** 883–99
[2] Vican J, Gajdeczko B F, Dryer F L, Milius F L, Aksay A and Yetter R A 2002 Development of a microreactor as a thermal source for MEMS power generation *Proc. Combust. Inst.* **29** 909–16
[3] Kim N I, Kato S, Kataoka T, Yokomori T, Maruyama S, Fujimori T and Maruta K 2005 Flame stabilization and emission of small Swiss-roll combustors as heaters *Combust. Flame* **141** 229–40
[4] Maruta K, Kataoka T, Kim N I, Minaev S and Fursenko R 2005 Characteristics of combustion in a narrow channel with a temperature gradient *Proc. Combust. Inst.* **30** 2429–36
[5] Pattekar A V and Kothare M V 2004 A microreactor for hydrogen production in micro fuel cell applications *J. Microelectromech. Syst.* **13** 7–18
[6] Ronney P D 2003 Analysis of non-adiabatic heat recirculating combustors *Combust. Flame* **135** 421–39
[7] Lloyd S A and Weinberg F J 1974 A burner for mixtures of very low heat content *Nature* **251** 47–8
[8] Epstein A H, Senturia S D and Anthasuresh G 1997 Power MEMS and microengines *IEEE Transducers '97 Conf. (Chicago, IL)* pp 753–6
[9] Mehra A, Zhang X, Ayon A A, Waitz I A, Schmidt M A and Spadaccini C M 2000 A six-wafer combustion system for a silicon micro gas turbine engine *J. Microelectromech. Syst.* **9** 517–27
[10] Spadaccini C M, Mehra A, Lee J, Zhang X, Lukachko and Waitz I A 2003 High power density silicon combustion system for micro gas turbine engines *J. Eng. Gas Turbines Power* **125** 709–19
[11] Mehra A 2000 Development of a high power density combustion system for a silicon micro gas turbine engine *PhD Thesis* Massachusetts Institute of Technology
[12] Hua J, Wu M and Kumar K 2005 Numerical simulations of the combustion of hydrogen air mixture in micro-scaled chambers: part II. CFD analysis for a micro combustor *Chem. Eng. Sci.* **60** 3507–15
[13] Wu M, Hua J and Kumar K 2005 An improved micro combustor design for micro gas turbine engine and numerical analysis *J. Micromech. Microeng.* **15** 1817–23
[14] Guidez J 2006 Study of the combustion in micro combustor for application to the micro gas turbine engines *Changes in Aeronautical and Space Systems: Challenges for On-Board Energy* (France: Avignon)
[15] Dumand C, Guidez J, Orain M and Sabel'nikov V A 2005 Specific problems of micro -turbine for micro-drones application *European Conference for Aerospace Sciences (Moscow)*
[16] Verstraete D and Trilla J 2006 Development of a combustion chamber for an ultra micro gas turbine *7th National Conference on Theoretical and Applied Mechanics (Mons, Belgium)*
[17] Kumar S, Maruta K and Minaev S 2007 Pattern formation of flames in radial microchannels with lean methane-air mixtures *Phys. Rev.* E **75** 016208
[18] Roy G, Nguyen C T and Lajoie P 2004 Numerical investigation of the laminar flow and heat transfer in a radial flow cooling system with the use of nanofluids *Superlattices Microstruct.* **35** 497–511
[19] Maruta K, Parc J K, Oh K C, Fujimori T, Minaev S S and Fursenko R V 2004 Characteristics of microscale combustion in a narrow heated channel *Combust. Explosion Shock Waves* **40** 516–23
[20] Kumar S, Maruta K and Minaev S 2007 On the formation of multiple rotating Pelton-like flame structures in radial microchannels with lean methane-air mixtures *Proc. Combust. Inst.* **31** 3261–8